

# Particle migration in planar die-swell flows

Ivan R. Siqueira<sup>1</sup> and Márcio S. Carvalho<sup>1,†</sup>

<sup>1</sup>Department of Mechanical Engineering, Pontifícia Universidade Católica do Rio de Janeiro,  
Rio de Janeiro, RJ 22451-900, Brazil

(Received 17 April 2017; revised 20 May 2017; accepted 25 May 2017;  
first published online 19 July 2017)

We present a numerical study on particle migration in a planar extrudate flow of suspensions of non-Brownian hard spheres. The suspension is described as a Newtonian liquid with a concentration-dependent viscosity, and shear-induced particle migration is modelled according to the diffusive flux model. The fully coupled set of nonlinear differential equations governing the flow is solved with a stabilized finite element method together with the elliptic mesh generation method to compute the position of the free surface. We show that shear-induced particle migration inside the channel leads to a highly non-uniform particle concentration distribution under the free surface. It is found that particle migration dramatically changes the shape of the free surface when the suspension is compared to a Newtonian liquid with the same bulk properties. Remarkably, we observed extrudate expansion in the Newtonian and dilute suspension flows; in turn, at high concentrations, a die contraction appears. The model does not account for normal stress differences, and this result is a direct consequence of variations in the flow stress field caused by shear-induced particle migration.

**Key words:** capillary flows, particle/fluid flow, suspensions

## 1. Introduction

Free-surface flows of particle suspensions play a key role in several industrial processes, such as continuous and discrete coatings, extrusion of plastics and fibres, and production of pharmaceutical and biomedical devices (Tadros 2011, 2017). The hydrodynamic interactions between the suspended particles in complex flows lead to shear-induced particle migration in the bulk of the suspension. As discussed in the comprehensive review of Stickel & Powell (2005), shear-induced particle migration drastically alters the flow characteristics when the suspension is compared to a Newtonian fluid with the same bulk properties and under the same conditions. Hence, fundamental understanding of the particle distribution in free-surface flows and the shape of the free surface itself is essential to process optimization.

Since the pioneering observations of Karnis, Goldsmith & Mason (1966) and Gadala-Maria & Acrivos (1980), a great effort has been made to better understand the phenomenon of shear-induced particle migration in the flow of concentrated

† Email address for correspondence: [msc@puc-rio.br](mailto:msc@puc-rio.br)

suspensions. The first discussion on the possibility of a cross-stream flux of particles is due to Leighton & Acrivos (1987), who used a simple scaling argument to develop a general expression for the diffusive flux of particles in unidirectional shear flows. They suggested that particle migration is based on irreversible particle–particle interactions because of gradients in frequency of particle interactions, particle concentration and effective suspension viscosity. As a consequence, the particles migrate against the direction of gradients in shear rate and suspension viscosity. The hypothesis for particle migration from high- to low-shear-rate regions was later confirmed by several experimental investigations of Poiseuille and cylindrical Couette flows (Husband & Gadala-Maria 1987; Abbott *et al.* 1991; Altobelli & Givler 1991; Graham & Altobelli 1991; Sinton & Chow 1991). Beyond these reports on particle migration in steady and fully developed conditions, other works have addressed particle migration in oscillatory flow fields. For instance, Butler, Majors & Bonnecaze (1999) used nuclear magnetic resonance imaging techniques to visualize shear-induced particle migration in oscillatory flows in a tube. A similar problem was studied numerically by Morris (2001) using Stokesian dynamics simulations. As a result, it was found that the migration towards the flow centreline is recovered at large oscillation amplitudes. In turn, at small amplitudes, the particles migrate towards the wall.

Phillips *et al.* (1992) extended the analysis of Leighton & Acrivos (1987) to develop a convection–diffusion equation that describes the evolution of particle concentration in the flow, establishing the now well-known diffusive flux model. The proposed theoretical model was validated through many experimental observations in cylindrical Couette and pressure-driven flows through tubes and channels using different experimental techniques (Koh, Hookham & Leal 1994; Hampton *et al.* 1997; Subia *et al.* 1998; Butler & Bonnecaze 1999; Han *et al.* 1999; Norman, Nayak & Bonnecaze 2005). However, the diffusive flux model presents some drawbacks. The model deals with some phenomenological parameters that are hard to measure (Graham, Mammoli & Busch 1998; Tetlow *et al.* 1998) and fails to predict particle migration in curvilinear torsional flows (Chapman 1990; Chow *et al.* 1994; Krishnan, Beimfohr & Leighton 1996; Bricker & Butler 2006; Kim, Lee & Kim 2008). Another difficulty of the model is related to the singularity that the particle transport equation presents in regions where the local shear rate vanishes, as occurs near the centreline of tubes and channel flows (Miller & Morris 2006; Ahmed & Singh 2011; Rebouças *et al.* 2016). Although it was developed strictly for one-dimensional shear flow, because of its relative simplicity, good accuracy and low computational cost, the diffusive flux model has been extensively used to predict particle concentration distributions in many problems of practical applications, such as flows with non-Newtonian continuous phase (Rao *et al.* 2002), evolving flows (Ingber *et al.* 2009), flows through asymmetric bifurcations (Ahmed & Singh 2011), flows of suspensions with non-spherical particles (Siqueira, Rebouças & Carvalho 2017a) and free-surface slot coating flows (Min & Kim 2010; Campana, Silva & Carvalho 2017; Siqueira, Rebouças & Carvalho 2017b).

Another approach typically used to study particle migration in suspension flows is the so-called suspension balance model, which was first proposed by Nott & Brady (1994) and then modified by Morris & Boulay (1999). The suspension balance model is a two-phase model which provides a continuum description of the bulk suspension motion, as well as the relative velocity of the particle phase and fluid phase. Its physical concept is that the migration phenomenon arises in order to balance a non-homogeneous normal stress because of the presence of the particles in the ambient Newtonian liquid. The particle flux is directly proportional to the

divergence of the particle stress tensor (i.e. an additional stress in the fluid-phase stress tensor), which includes contact or interparticle effects as well as hydrodynamic contributions. Recently, Snook, Butler & Guazzelli (2016) considered refractive index matching techniques to investigate the dynamics of shear-induced particle migration in oscillatory pipe flows and compared the experimental results with the predictions of the suspension balance model using rheological models (Morris & Boulay 1999; Boyer, Pouliquen & Guazzelli 2011*b*). Nevertheless, the suspension balance model requires correlations for the particle-phase stress which cannot be easily obtained experimentally (Zarraga, Hill & Leighton 2000; Boyer, Pouliquen & Guazzelli 2011*a*; Couturier *et al.* 2011; Dbouk, Lobry & Lemaire 2013), and the exact nature of the particle stress that is responsible for particle migration is still a subject of debate (Lhuillier 2009; Nott, Guazzelli & Pouliquen 2011).

The first experimental report about particle migration in free-surface flows is the work of Husband *et al.* (1994), who performed an extensive investigation on the flow of bimodal suspensions along an inclined plane. They found that the particles migrate to the low-shear-rate region near the air–liquid interface. Moreover, they also verified that large particles migrate with a higher rate than the small ones, leading to a size segregation in the flow. Tirumkudulu, Tripathi & Acrivos (1999) and Tirumkudulu, Mileo & Acrivos (2000) considered the flow of a monodisperse suspension of neutrally buoyant spherical particles in a partially filled rotating cylinder. They observed that the suspension segregates into regions of high and low particle concentration along the cylinder axis, and that the particle concentration fluctuations lead to an instability in the flow (Govindarajan, Nott & Ramaswamy 2001; Timberlake & Morris 2002; Jin & Acrivos 2004). Loimer, Nir & Semiat (2002) studied the free-surface topography along the vorticity direction in simple shear flows of concentrated suspensions. They noticed that the roughness of the surface disturbances depends on the particle size, particle concentration and the surface tension of the suspending fluid. Free-surface topography was also investigated in gravity-driven flows of concentrated suspensions along an inclined plane by Timberlake & Morris (2005) and Singh, Nir & Semiat (2006).

Recently, some numerical analyses have been developed to investigate particle migration in free-surface flows using the diffusive flux model. For instance, Min & Kim (2010) used the finite volume method together with the volume of fluid model to investigate particle migration in two free-surface flows of particle suspensions. They presented a first discussion on the effects of inertia, particle size and suspension bulk concentration on the flow characteristics. Campana *et al.* (2017) studied slot coating flows of particle suspensions using the finite element method, and showed that the final particle distribution in the coated film is not uniform and depends strongly on the operating parameters. A similar study was conducted by Siqueira *et al.* (2017*b*) considering particle alignment in slot coating flows of suspensions of non-spherical particles. The effect of particle fillers in different process flows with free surfaces has been studied experimentally. Chu *et al.* (2006) reported changes in the operability window of the slot coating process associated with suspended inorganic particles in poly(vinyl alcohol) solutions. Liang (2010) showed that the extrudate swell of polypropylene composites containing diatomite particles decreases as the particle volume fraction rises. Die swell in the polypropylene polymer matrix was suppressed by the addition of carbon nanotubes, as reported by Kharchenko *et al.* (2004). However, the mechanisms by which the suspended particles affect die-swell flows of particle suspensions are still not clear.

In this work, we perform a detailed numerical study on shear-induced particle migration in planar die-swell flows of particle suspensions, exploring a wide range of

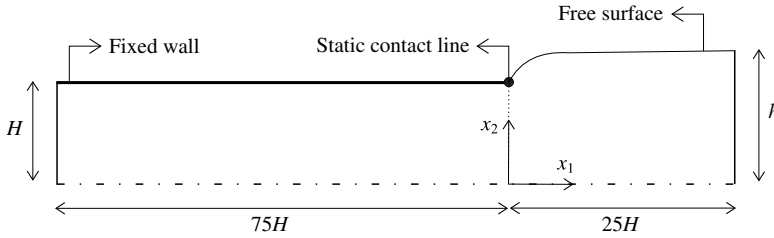


FIGURE 1. A schematic diagram of the geometry of the problem (not to scale).

model parameters and examining the effects of particle migration in the free-surface configuration. The suspension is assumed to be composed by non-Brownian spherical particles dispersed in a Newtonian liquid, and particle migration is described according to the diffusive flux model. The set of governing equations is solved numerically by a stabilized finite element method together with the elliptic mesh generation method to compute the position of the free surface. The rest of this article is organized as follows. The mathematical model is described in § 2, and the numerical methodology employed is reviewed in § 3. Then, § 4 is devoted to the numerical results and discussions. Finally, some concluding remarks are presented in § 5.

## 2. Mathematical formulation

The liquid flows through a channel between two parallel plates and then is extruded into the ambient atmosphere. A sketch of the geometry of the problem is shown in figure 1, where  $H$  is half of the channel gap. The free-surface height  $h$  is unknown *a priori* and depends on the flow parameters. The lengths of the inlet channel and free-surface region were chosen to be  $75H$  and  $25H$ , respectively. The flow is assumed to be symmetric with respect to the  $x_2 = 0$  plane. Therefore, only the upper half of the channel is considered. It is worth mentioning that particle migration does not reach a fully developed condition at the end of the upstream channel. As discussed by Nott & Brady (1994), the channel length necessary to obtain a fully developed particle concentration distribution is very high. However, the geometry used here is long enough to lead to a strongly non-uniform particle concentration field and consequently to viscosity gradients that change the flow behaviour, as discussed in the results section.

Because of the typical scales involved in the problem, i.e. the particle diameter is much smaller than the channel height, the suspension can be treated as an equivalent continuum liquid in the flow domain. Under this circumstance, the flow is governed by incompressible mass conservation and momentum conservation equations, namely

$$\nabla \cdot \mathbf{u} = 0 \quad (2.1)$$

and

$$\rho \left( \frac{\partial \mathbf{u}}{\partial t} + \mathbf{u} \cdot \nabla \mathbf{u} \right) = \nabla \cdot \boldsymbol{\Sigma} + \rho \mathbf{g}. \quad (2.2)$$

In (2.1) and (2.2),  $\mathbf{u}$  is the velocity field vector,  $\rho$  is the suspension density,  $\boldsymbol{\Sigma}$  is the suspension stress tensor and  $\mathbf{g}$  is the gravitational field vector. The stress tensor is split as  $\boldsymbol{\Sigma} = -p\mathbf{l} + \boldsymbol{\tau}$ , where  $p$  is the pressure field,  $\mathbf{l}$  is the unit tensor and  $\boldsymbol{\tau}$  is the extra-stress tensor field.

We assume that the extra-stress is a purely viscous stress that obeys Newton's law with a concentration-dependent viscosity, such that  $\boldsymbol{\tau} = \eta \dot{\boldsymbol{\gamma}}$ , where  $\eta = \eta(\phi)$  is the suspension viscosity,  $\phi$  is the local particle concentration and  $\dot{\boldsymbol{\gamma}} = \nabla \mathbf{u} + \nabla \mathbf{u}^T$  is the rate-of-strain tensor, in which the superscript T denotes the transpose operation. The suspension viscosity is given by a differential-effective-medium-based model recently proposed by Santamaría-Holek & Mendoza (2010), such that

$$\eta = \eta_0 \left[ 1 - \left( \frac{\phi}{1 - c\phi} \right) \right]^{-[\eta]}, \quad (2.3)$$

where  $\eta_0$  is the viscosity of the Newtonian solvent liquid,  $[\eta]$  is the so-called intrinsic viscosity and  $c = (1 - \phi_c)/\phi_c$  is a crowding factor that guarantees that the particles cannot occupy all the volume of the sample due to geometric restrictions, in which  $\phi_c$  is the critical particle concentration at which the suspension loses its fluidity, i.e.  $\eta \rightarrow \infty$  as  $\phi \rightarrow \phi_c$ . For suspensions of hard spheres, it follows that  $[\eta] = 2.5$  and  $\phi_c = 0.637$ . It is worth mentioning that (2.3) recovers the classical result of Einstein (1911) at the limit of infinitely dilute suspensions, and provides good results when compared to experimental data over the entire concentration range.

Because of irreversible particle–particle interactions that occur in non-uniform shear flows, the suspended particles tend to migrate to preferred regions in the flow domain. Shear-induced particle migration is described by the diffusive flux model developed by Phillips *et al.* (1992). The model states a typical convection–diffusion equation accounting for particle transport in the flow, such that

$$\frac{\partial \phi}{\partial t} + \mathbf{u} \cdot \nabla \phi = -\nabla \cdot \mathbf{N}_\phi, \quad (2.4)$$

where  $\mathbf{N}_\phi$  is the total diffusive flux of particles due to different mechanisms. Initially, Phillips *et al.* (1992) recognized that particle migration arises from two different mechanisms, namely gradients in shear rate and gradients in suspension viscosity. They used the theory of Leighton & Acrivos (1987) to develop mathematical expressions for these two fluxes, as follows:

$$\mathbf{N}_c = -K_c a^2 \phi \nabla (\dot{\gamma} \phi) \quad (2.5)$$

and

$$\mathbf{N}_\eta = -K_\eta a^2 \left( \frac{\dot{\gamma} \phi^2}{\eta} \right) \nabla \eta, \quad (2.6)$$

where  $\mathbf{N}_c$  and  $\mathbf{N}_\eta$  are the diffusive flux of particles because of gradients in shear rate and gradients in suspension viscosity, respectively. In (2.5) and (2.6),  $\dot{\gamma} = |\dot{\boldsymbol{\gamma}}|$  is the local shear rate (i.e. the second invariant of the rate-of-deformation tensor),  $a$  is the particle radius, and the parameters  $K_c$  and  $K_\eta$  are diffusion-like coefficients inherent to the model that should be found from experimental results. We set  $K_c = 0.41$  and  $K_\eta = 0.62$ , as found by Phillips *et al.* (1992) in pressure-driven flows through tubes and cylindrical Couette flows. We also consider an additional diffusive flux of particles because of the curvature of the streamlines in the flow, as introduced by Krishnan *et al.* (1996) and later adapted by Kim *et al.* (2008) to a frame-independent formulation. The mathematical expression for this flux is

$$\mathbf{N}_\kappa = K_\kappa a^2 \dot{\gamma} \phi^2 \boldsymbol{\kappa} \mathbf{n}_s, \quad (2.7)$$

where  $\kappa$  is the local radius of curvature of a streamline and  $\mathbf{n}_s$  is the unit normal vector in the radially outward direction of a curved streamline. Following Kim *et al.* (2008), the additional diffusion-like coefficient is defined as  $K_\kappa = K_c$ . It is worth mentioning that we are considering suspensions of neutrally buoyant particles, so that the effects related to sedimentation because of gravity are neglected, and the suspension density is equal to the density of the Newtonian solvent liquid.

The boundary conditions used to solve (2.1), (2.2) and (2.4) are given below, in which  $\mathbf{n}$  and  $\mathbf{t}$  are local unit normal and tangent vectors to the boundaries, respectively.

- (i) Synthetic inflow plane: At the inflow plane, we assume a uniform particle concentration,  $\phi = \bar{\phi}$ , where  $\bar{\phi}$  is the suspension bulk concentration, and a fully developed, parabolic velocity profile, so that

$$\mathbf{u} = \frac{3}{2}V \left[ 1 - \left( \frac{x_2}{H} \right)^2 \right] \hat{\mathbf{e}}_1, \quad (2.8)$$

where  $V = Q/H$  is the flow mean velocity and  $Q$  is the imposed flow rate (per unit width).

- (ii) Symmetry plane: Because of symmetry, we have that  $\mathbf{n} \cdot \mathbf{u} = 0$ ,  $\mathbf{t} \cdot (\mathbf{n} \cdot \boldsymbol{\Sigma}) = 0$  and  $\mathbf{n} \cdot \mathbf{N}_\phi = 0$  along the flow centreline.
- (iii) Synthetic outflow plane: At the outflow plane, we assume a fully developed velocity profile with an imposed pressure,  $\mathbf{n} \cdot \nabla \mathbf{u} = 0$  and  $p = 0$ . Moreover, there is no diffusive flux of particles, such that  $\mathbf{n} \cdot \mathbf{N}_\phi = 0$ .
- (iv) Free surface: At the free surface, the shear stress vanishes and there is no liquid flux across the air–liquid interface, so that  $\mathbf{t} \cdot (\mathbf{n} \cdot \boldsymbol{\Sigma}) = 0$  and  $\mathbf{n} \cdot \mathbf{u} = 0$ . Moreover, the liquid traction should balance the sum of the pressure in the external gas and the capillary pressure induced by the curvature of the free surface. The stress jump across the interface is written as  $\mathbf{n} \cdot \boldsymbol{\Sigma} = (-p_g + \sigma\kappa)\mathbf{n}$ , where  $p_g = 0$  is the external gas pressure,  $\sigma$  is the suspension surface tension and  $\kappa$  is the curvature of the free surface. The liquid surface tension is assumed to be constant and independent of the local particle concentration at the interface, such that there are no Marangoni effects (Chandrasekhar 1961). Finally, we also assume that there is no adsorption or desorption of particles in the free surface, which leads to  $\mathbf{n} \cdot \mathbf{N}_\phi = 0$ .
- (v) Static contact line: The contact line is pinned at the corner of the channel exit.

A dimensional analysis of the problem suggests that it is convenient to introduce three dimensionless numbers, which are combinations of the various macroscopic model parameters. These dimensionless numbers are: (i) the macroscopic Reynolds number,  $Re = \rho Q/\bar{\eta}$ ; (ii) the capillary number,  $Ca = \bar{\eta}V/\sigma$ ; and (iii) the ratio of particle radius to channel gap,  $\zeta = a/H$ . Here,  $\bar{\eta} = \eta(\bar{\phi})$  is the average suspension viscosity evaluated with the bulk concentration  $\bar{\phi}$ , i.e. neglecting particle migration. All simulations were performed at  $Re = 0$ ,  $a = 100 \mu\text{m}$  and  $\zeta = 10^{-1}$ , so that the only parameters that are varied in this work are  $Ca$  and  $\bar{\phi}$ .

### 3. Numerical method

Because of the free surface, the domain of the extrudate swell flow analysed here is not known *a priori*. The domain is part of the solution and depends on the flow parameters. In order to solve this free-boundary flow by means of standard techniques for fixed domain problems, the set of equations and boundary conditions posed in the

unknown domain (i.e. the physical domain) have to be transformed to an equivalent problem defined in a known domain (i.e. a reference computational domain). This transformation is made by a mapping  $\mathbf{x} = \mathbf{x}(\boldsymbol{\xi})$  that connects the two domains. The mapping procedure used here is based on the elliptic mesh generation method presented by Christodoulou (1990) and de Santos (1991). In this case, the inverse mapping satisfies an elliptic equation identical to those encountered in diffusion transport with variable diffusion coefficients,

$$\nabla \cdot (\mathcal{D} \nabla \boldsymbol{\xi}) = \mathbf{0}, \quad (3.1)$$

where  $\boldsymbol{\xi}$  is the position vector in the computational domain and  $\mathcal{D}$  is a symmetric positive definite second-order tensor of diffusion-like coefficients used to control element spacing in the reference domain (Benjamin 1994). Equation (3.1) is usually referred to as the mesh generation equations. Boundary conditions are also needed to solve the second-order partial differential equations of mesh generation. The solid boundaries and the synthetic inflow and outflow planes are defined by functions of the coordinates in the physical domain, and stretching functions are used to distribute the nodes along the boundaries. At the static contact line, either the position of the contact line is specified, or the angle between the unit normal vector outwards from the free surface and the unit normal vector outwards from the solid boundary is fixed, and the contact line lies on the solid boundary. Here, we kept the position of the contact line fixed at  $\mathbf{x}/H = (0, 1)$ , so that the contact angle is part of the solution of the problem. The position of the free surface is implicitly defined by the kinematic condition  $\mathbf{u} \cdot \mathbf{n} = 0$ , such that there is no liquid flux across the air–liquid interface. This version of the elliptic mesh generation method has been widely used in numerical simulations of free-surface flows, such as coating flows of Newtonian liquids (Carvalho & Scriven 1997; Carvalho & Khesghi 2000; Tjiptowidjojo & Carvalho 2011), non-Newtonian polymer solutions (Pasquali & Scriven 2002; Romero *et al.* 2004; Romero, Scriven & Carvalho 2006; Bajaj, Prakash & Pasquali 2008) and particle suspensions (Campana *et al.* 2017; Siqueira *et al.* 2017*b*), stretching of liquid bridges (Dodds, Carvalho & Kumar 2009, 2011, 2012) and predictions of dynamic wetting failure (Vandre, Carvalho & Kumar 2012, 2013, 2014; Liu *et al.* 2016).

Numerical approximations of the transport equations and the mesh generation equations were obtained by using the DEVSS-TG/SUPG mixed finite element method (Guénette & Fortin 1995; Szady *et al.* 1995; Pasquali & Scriven 2002). The DEVSS-TG formulation treats the velocity gradient as an independent variable with a traceless continuous interpolation. The interpolated velocity gradient is then used to compute the viscous stress with a discrete adaptive split. The independent variables of the problem are written as a linear combination of a finite number of basis functions. Lagrangian biquadratic functions represent the velocity field, particle concentration and mesh position; Lagrangian bilinear functions represent the interpolated velocity gradient; and linear discontinuous functions are used for the pressure field. Galerkin weighting functions are used in the residual equations of mass conservation, momentum conservation, mesh position and interpolated velocity gradient, and the streamline-upwinding Petrov–Galerkin formulation is applied in the particle transport equation. In addition to that, the singularity of the diffusive flux model was treated with a modified version of the non-local stress contribution to the shear rate presented by Rebouças *et al.* (2016). The result is a large, sparse set of coupled, nonlinear algebraic equations, which was solved using Newton's method with a numerical Jacobian matrix obtained with a second-order central difference scheme.

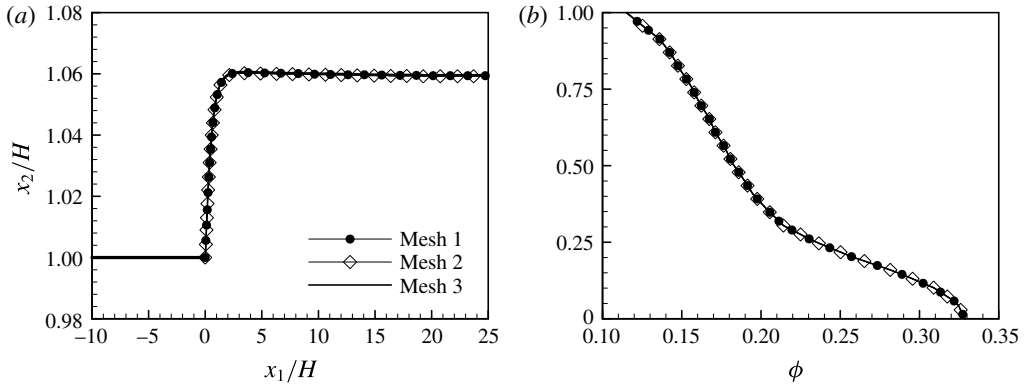


FIGURE 2. Mesh independence test: (a) position of the free surface; (b) particle concentration distribution at the outflow plane ( $x_1/H = 25$  plane). Simulations at  $Ca = 2.5$  and  $\bar{\phi} = 0.20$ .

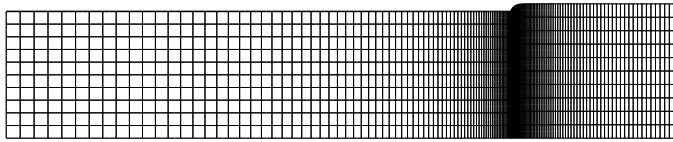


FIGURE 3. Representative mesh used in the simulations (not to scale).

---

Mesh	Elements	Nodes	DoFs
Mesh 1	1000	4221	28 594
Mesh 2	1250	5271	35 649
Mesh 3	1500	6321	42 749

---

TABLE 1. Mesh information

The tolerance on the  $L^2$ -norm of the global residual vector and Newton's update was set to  $10^{-6}$ . At each iteration, the linear system was solved with a frontal solver based on the LU factorization method (Duff, Erisman & Reid 1989), and solutions at different parameters were obtained with a first-order arclength continuation (Bolstad & Keller 1986).

We performed a grid-independence study for a representative combination of the governing parameters to ensure that the numerical results are independent of the mesh refinement. Three different meshes were examined, and the number of elements, nodes and degrees of freedom (DoFs) of each one of them is specified in table 1. The accuracy of our approximations was assured by computing the shape of the free surface and the particle concentration distribution at the free-surface outflow plane ( $x_1/H = 25$  plane). These results are presented in figure 2. In this test, we have used  $Ca = 2.5$  and  $\bar{\phi} = 0.20$ . As can be seen, the three meshes yield quite close results. Mesh 3, illustrated in figure 3, was selected and employed for all cases investigated.



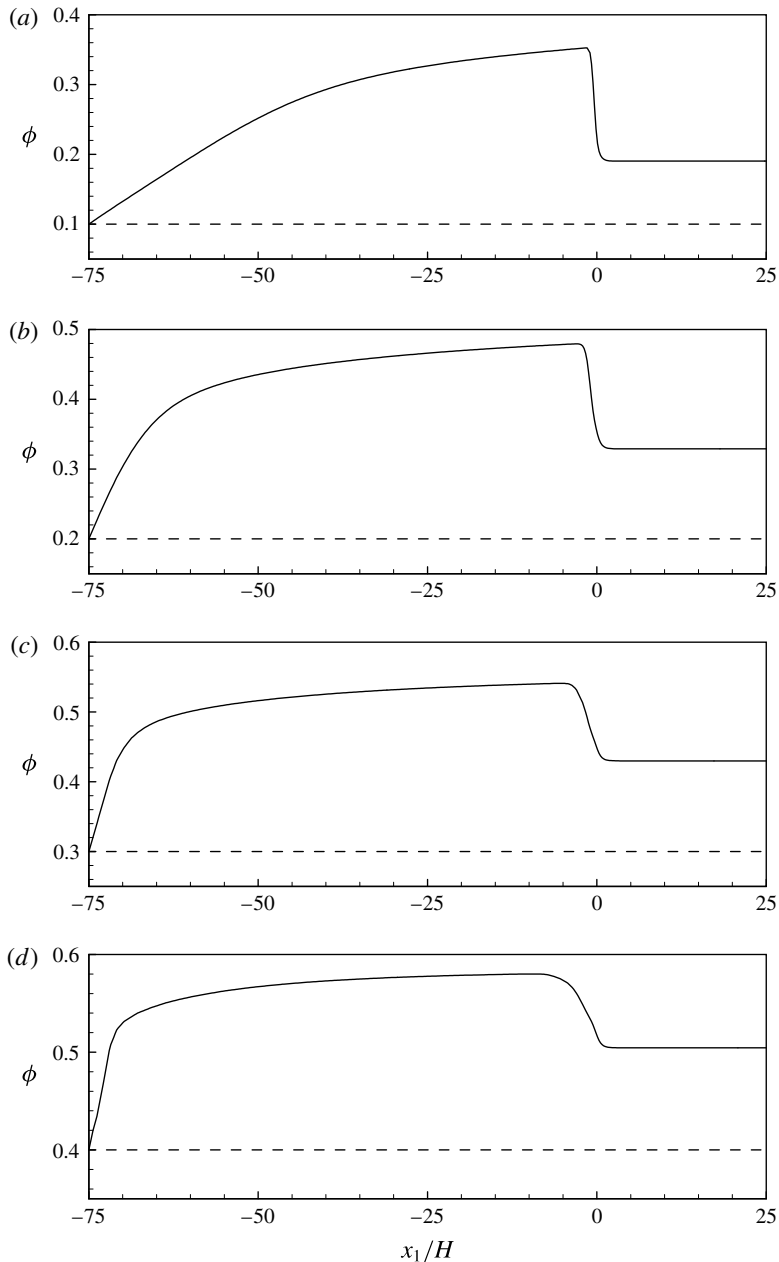


FIGURE 4. Particle concentration along the flow centreline ( $x_2/H = 0$  plane) for: (a)  $\bar{\phi} = 0.10$ ; (b)  $\bar{\phi} = 0.20$ ; (c)  $\bar{\phi} = 0.30$ ; (d)  $\bar{\phi} = 0.40$ . Simulations at  $Ca = 1$ .

#### 4. Results and discussion

First, we investigate particle migration by examining the particle concentration along the flow centreline. Figure 4 shows the results for suspensions at different bulk concentrations at  $Ca = 1$ . As expected, particle concentration along the centreline increases as the suspension flows inside the channel. Indeed, particles migrate from

regions of high shear rate near the wall to regions of low shear rate near the symmetry plane. Particle concentration reaches a maximum value close to the end of the channel. For  $\bar{\phi} = 0.10$ , the maximum concentration is  $\phi_m \approx 0.35$  and occurs at  $x_1/H \approx -1.5$ , and for  $\bar{\phi} = 0.40$  it is  $\phi_m \approx 0.58$  and occurs at  $x_1/H \approx -8.1$ . Just before the exit of the channel, the centreline concentration shows a sudden decrease, which is a consequence of the transition from the bounded flow inside the channel to the free-surface flow outside the channel. At the intersection between the channel and the free surface, the shear rate undergoes a rapid variation from a maximum value at the channel wall to zero at the air–liquid interface. Therefore, the free-surface induces a redistribution in the particle concentration field near the channel exit, pushing the particles towards the air–liquid interface and thereby decreasing the centreline concentration. However, for  $x_1/H \gtrsim 1$ , the centreline concentration along the free surface remains constant and higher than the suspension bulk concentration. For  $\bar{\phi} = 0.10$ , the concentration along the free-surface centreline is  $\phi_{cfs} \approx 0.19$ , and for  $\bar{\phi} = 0.40$  it is  $\phi_{cfs} \approx 0.50$ .

The constant concentration along the free-surface centreline shows that shear-induced particle migration is almost negligible in the flow under the free surface. The flow in that region is bounded by the flow symmetry plane and the air–liquid interface, and since the shear rate vanishes along these two boundaries, the gradient in shear rate is almost zero, i.e. the flow approaches a plug flow condition. The constant centreline concentration under the free surface is greater than the suspension bulk concentration,  $\phi_{cfs} > \bar{\phi}$ , which indicates the existence of gradients in particle concentration in the extrudate. Thus, particle migration in this region arises only from gradients in suspension viscosity and curved streamlines. However, as discussed by Nott & Brady (1994), the diffusive mechanisms are relatively weak, so that particle migration under the free surface is very slow. Figure 5 displays the particle concentration distribution at the outflow plane. In all cases, particle concentration is higher near the flow centreline, and drastically decreases towards the air–liquid interface. For  $\bar{\phi} = 0.10$ , the interface concentration is  $\phi_i \approx 0.06$ , and for  $\bar{\phi} = 0.40$  it is  $\phi_i \approx 0.27$ . Figure 6 shows the particle concentration field in the entire flow domain, highlighting the non-uniform distribution of particle concentration inside the channel and under the free-surface region.

In all plots presented in figure 5 the  $x_2$  coordinate in the free jet was normalized by the free jet final height,  $h$ . However, the free-surface height and the shape of the free surface itself depend strongly on the flow parameters, as can be seen in figure 6. For a circular die at the limit of small Reynolds number, the interface swells to approximately 13% of the tube diameter in the case of Newtonian liquids. In the case of polymeric solutions, the extrudate swell can be as high as 300%. This difference in the extrudate diameter is related to the presence of normal stress differences in polymeric liquids (Tanner 1985; Bird, Armstrong & Hassager 1987). Normal stress differences in the flow of non-colloidal suspensions can be computed if the suspension balance model of Nott & Brady (1994) and Morris & Boulay (1999) is used. However, the diffusive flux model together with the constitutive equation used here does not show normal stress difference, i.e.  $N_1 = N_2 = 0$ . Therefore, the predicted variation of the extrudate swell is related to the non-uniform particle distribution in the flow due to shear-induced migration. Figure 7 compares the shape of the free surface of suspensions with different bulk concentrations (but with the same average bulk viscosity) and a Newtonian liquid with the same average bulk properties. The extrudate final height decreases considerably as the suspension concentration increases. At low concentrations, the extrudate height is smaller than that of the Newtonian flow.

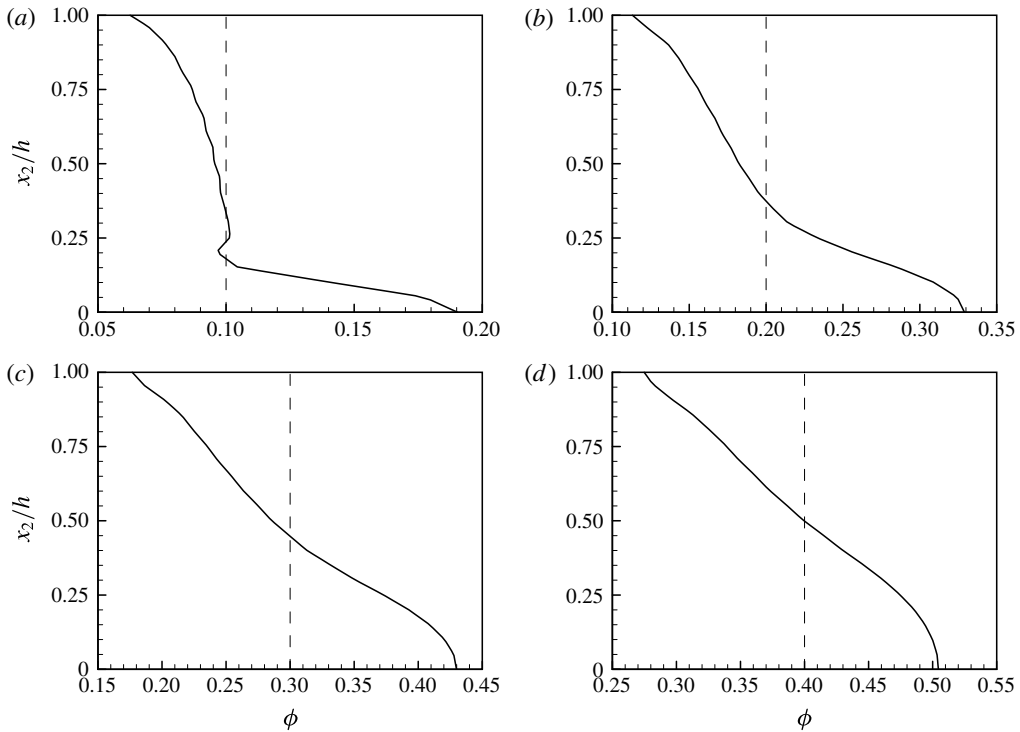


FIGURE 5. Particle concentration distribution at the free-surface outflow plane ( $x_1/H = 25$  plane) for: (a)  $\bar{\phi} = 0.10$ ; (b)  $\bar{\phi} = 0.20$ ; (c)  $\bar{\phi} = 0.30$ ; (d)  $\bar{\phi} = 0.40$ . Simulations at  $Ca = 1$ .

For the Newtonian liquid,  $h/H \approx 1.13$ , and for  $\bar{\phi} = 0.10$  and  $\bar{\phi} = 0.20$ , we found  $h/H \approx 1.11$  and  $h/H \approx 1.05$ , respectively. In turn, at high concentrations, the extrudate height is smaller than the channel gap; at  $\bar{\phi} = 0.30$ ,  $h/H \approx 0.99$ , and at  $\bar{\phi} = 0.40$ ,  $h/H \approx 0.95$ .

Inside the channel, particles are concentrated near the symmetry plane and the wall layer is depleted of particles, which leads to a very intense viscosity gradient in the flow. Therefore, the velocity profile of the suspension flow at the channel exit is blunted when compared to the Newtonian liquid. As the suspension concentration increases, the viscosity near the centreline increases and thereby the centreline velocity decreases; in turn, the viscosity near the wall decreases, leading to a higher velocity gradient in this region. This result is shown in figure 8(a). Figure 8(b) shows the fluid velocity along the symmetry plane, and figure 9 displays the horizontal velocity field in the entire flow domain. For the Newtonian case, the centreline velocity inside the channel is constant and equal to  $u/V = 1.5$ , and experiences a sudden decrease to  $u/V \approx 0.88$  as the free surface approaches. Since  $u/V < 1$  under the free surface, the flow decelerates and we observe a die expansion with respect to the channel gap in order to satisfy mass conservation. When particle migration is considered in the suspension flow, the particles are more concentrated near the flow centreline, such that the high viscosity in this region leads to a decrease in the centreline velocity. At  $\bar{\phi} = 0.10$ , the centreline velocity decreases from  $u/V \approx 1.49$  inside the channel to  $u/V \approx 0.91$  along the free surface. So, there is also a die expansion, but with an extrudate height smaller than the Newtonian case. At  $\bar{\phi} = 0.40$ , the centreline concentration is so

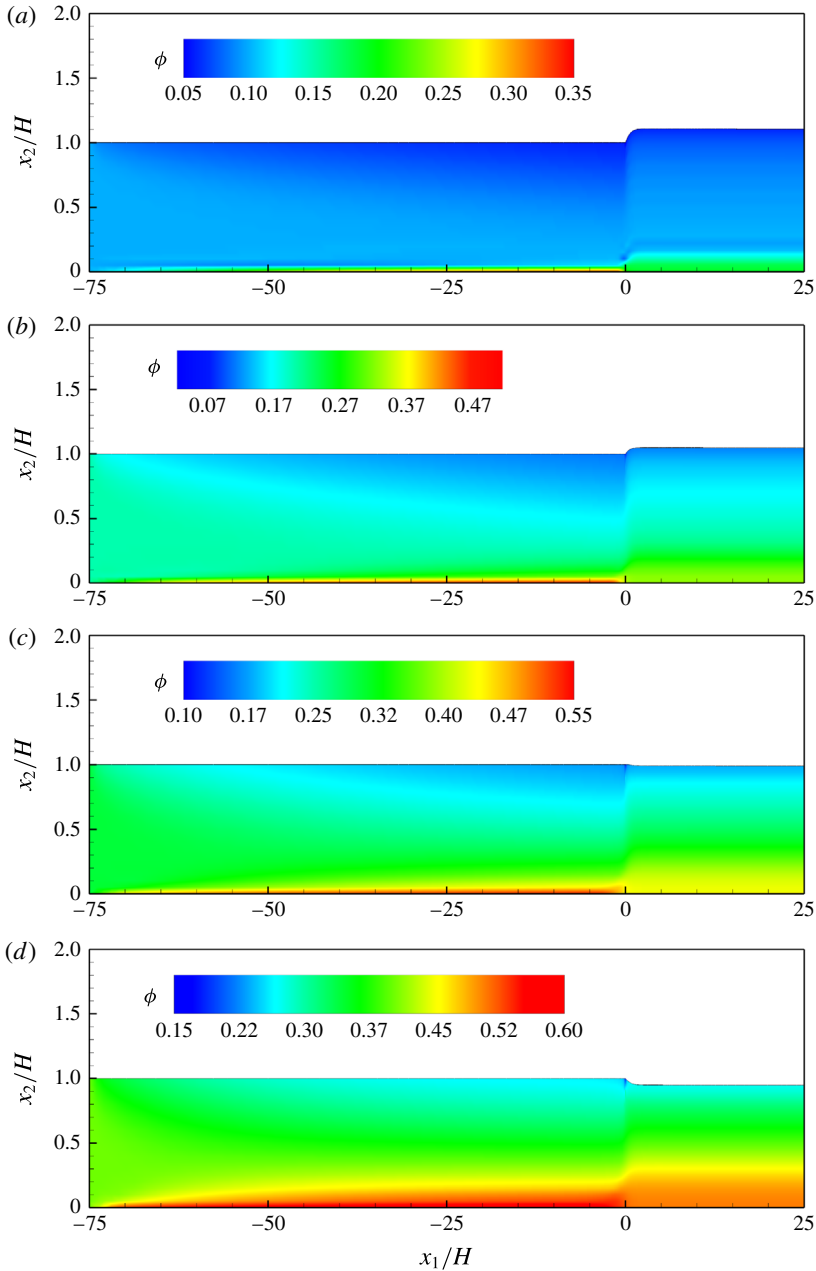


FIGURE 6. (Colour online) Particle concentration field in the flow domain for: (a)  $\bar{\phi} = 0.10$ ; (b)  $\bar{\phi} = 0.20$ ; (c)  $\bar{\phi} = 0.30$ ; (d)  $\bar{\phi} = 0.40$ . Simulations at  $Ca = 1$ .

high that the velocity falls from  $u/V \approx 1.37$  inside the channel to  $u/V \approx 1.05$  in the free surface. Since  $u/V > 1$  under the free surface, the extrudate velocity is higher than the flow mean velocity and a die contraction appears in order to satisfy mass balance. There are a few experimental reports on extrudate contraction in the flow of concentrated suspensions. Aral & Kalyon (1997) presented evidence on a variation

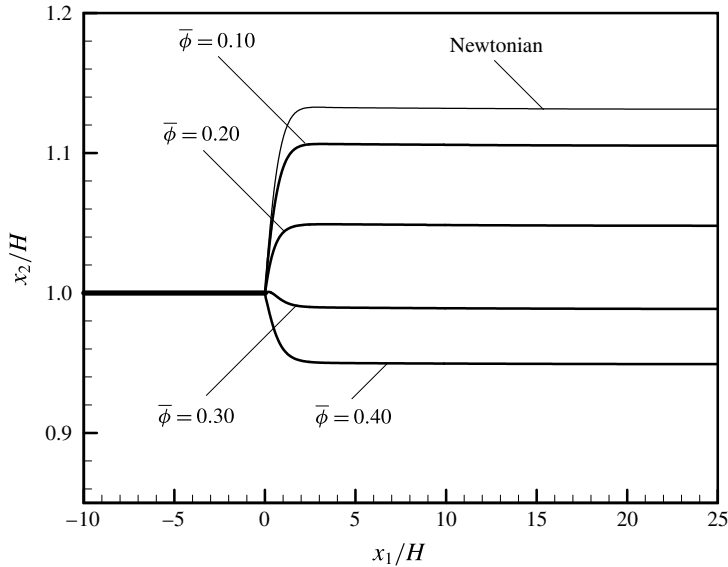


FIGURE 7. Shape of free surface. Simulations at  $Ca = 1$ .

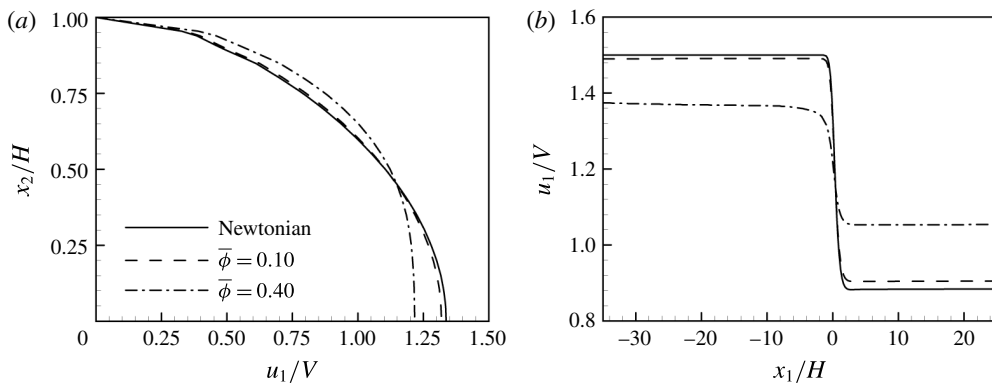


FIGURE 8. Comparison of the velocity field in the flow of suspensions and a Newtonian liquid: (a) velocity profile at the channel exit ( $x_1/H = 0$  plane); (b) centreline velocity at the free surface ( $x_2/H = 0$  plane). Simulations at  $Ca = 1$ .

in extrudate shape in the flow of dense suspensions of non-colloidal spheres. Nicolas (2002) observed a die contraction in gravity-driven jets of concentrated suspensions. A qualitatively similar result was reported by Furbank & Morris (2004) on the formation of drops of particulate suspensions. However, in the works of Nicolas (2002) and Furbank & Morris (2004), both inertial and gravitational effects were not negligible, so that we cannot be sure whether the die contraction they observed was caused by the same mechanism as discussed here. Extrudate contraction was also reported by Kharchenko *et al.* (2004) in the flow of concentrated suspensions of carbon nanotubes, which was assumed to be a consequence of particle alignment in the flow direction.

The variations in suspension viscosity and flow velocity caused by particle migration imply a strong change in the suspension stress field near the channel exit and the

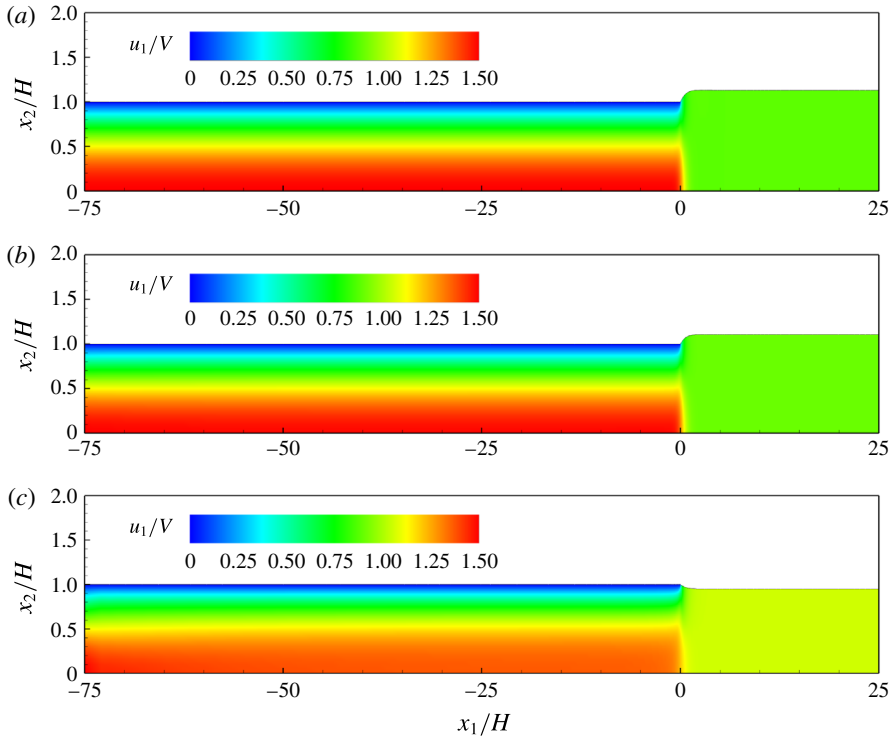


FIGURE 9. (Colour online) Horizontal velocity field in the entire flow domain for: (a) Newtonian liquid; (b)  $\bar{\phi} = 0.10$ ; (c)  $\bar{\phi} = 0.40$ . Simulations at  $Ca = 1$ .

entrance of the free-surface region. Figure 10 compares the stress field in this region for a Newtonian fluid, a dilute suspension at  $\bar{\phi} = 0.10$  and a concentrated suspension at  $\bar{\phi} = 0.40$ . In all cases, the fluids present the same average bulk viscosity. In these plots, the stress components are evaluated in units of  $\tau_c = \bar{\eta}V/H$ , the characteristic shear stress of the flow. The normal stress  $\Sigma_{22}$  along the  $x_2 = 0$  plane rises as the suspension bulk concentration increases. The resulting vertical net force along the plane is compressive for the Newtonian fluid. Therefore, the vertical component of the surface tension force acting at the contact line needs to be negative in order to satisfy momentum balance; the free-surface height is larger than the channel gap. On the other hand, the resulting vertical net force along the plane pulls the liquid downwards for the concentrated particle suspension at  $\bar{\phi} = 0.40$ . The vertical component of the surface tension force at the contact line needs to be positive, resulting in an extrudate contraction. This stress-based argument explains the change in the free-surface curvature from a Newtonian liquid and dilute suspensions, where a die expansion is observed, to concentrated suspensions, where a die contraction appears.

In the absence of inertia and gravity, the shape of the free surface is dictated by a balance between viscous and interfacial forces near the air–liquid interface, which is represented by the flow capillary number. Figure 11 shows the effect of the capillary number on the free jet final height. In all cases, the flow rate was kept fixed and the capillary number was varied only by changing the liquid surface tension. At very low capillary number, the flow is dominated by surface-tension forces, which act in the

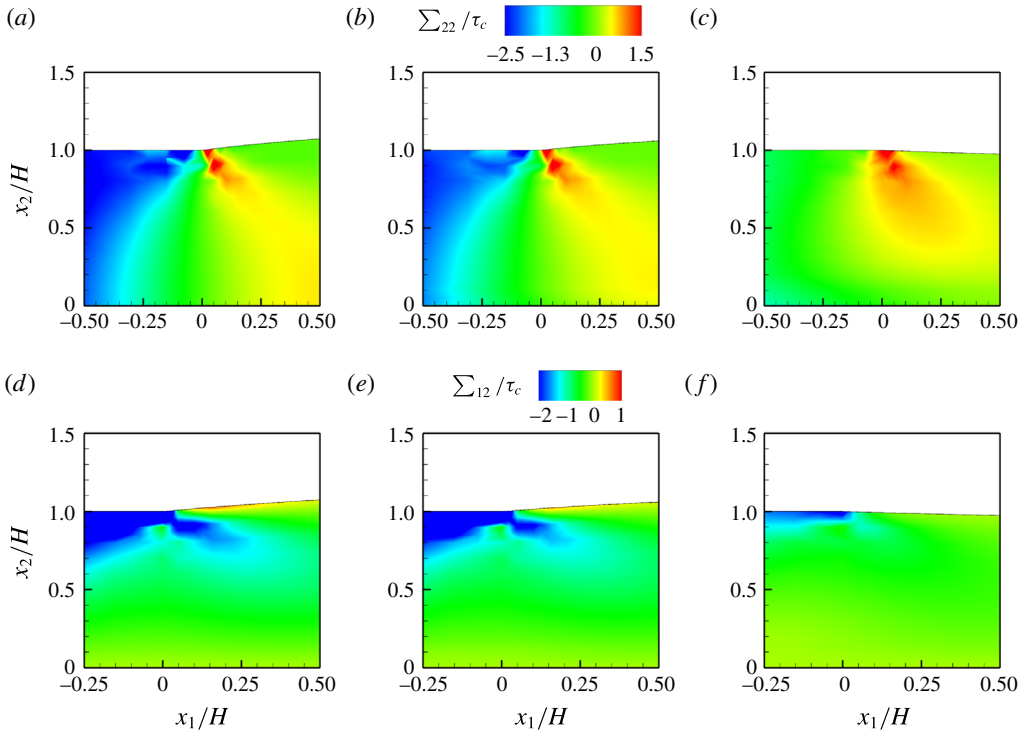


FIGURE 10. (Colour online) Stress field near the entrance of the free surface. (a–c) For  $\Sigma_{22}/\tau_c$ : (a) Newtonian liquid; (b)  $\bar{\phi} = 0.10$ ; (c)  $\bar{\phi} = 0.40$ . (d–f) For  $\Sigma_{12}/\tau_c$ : (d) Newtonian liquid; (e)  $\bar{\phi} = 0.10$ ; (f)  $\bar{\phi} = 0.40$ . Simulations at  $Ca = 1$ .

sense to avoid the curvature of the free surface. As a consequence, the extrudate final height is almost equal to the channel gap, i.e.  $h/H \approx 1$ , without a considerable die expansion or contraction. At  $Ca = 10^{-2}$ ,  $h/H \approx 1.005$  for the Newtonian liquid,  $h/H \approx 1.002$  for suspensions at  $\bar{\phi} = 0.10$  and  $h/H \approx 0.995$  for suspensions at  $\bar{\phi} = 0.40$ . As the capillary number increases and viscous effects become dominant, the free-surface curvature increases in order to balance the viscous force at the air–liquid interface. Therefore, the extrudate final height and the die expansion increase in the case of a Newtonian liquid and suspensions at low concentrations. In turn, the free jet final height decreases and the die contraction becomes more pronounced for suspensions at high concentrations. At the limit of very high capillary number, the relation  $h/H$  tends to a constant asymptotic value. At  $Ca = 10^2$ ,  $h/H \approx 1.189$  for the Newtonian liquid,  $h/H \approx 1.149$  for suspensions at  $\bar{\phi} = 0.10$  and  $h/H \approx 0.936$  for suspensions at  $\bar{\phi} = 0.40$ . Although the capillary number has a strong effect on the extrudate shape, we verified that it has a negligible effect on the final particle distribution at the free-surface outflow plane when the  $x_2$  coordinate is normalized by the corresponding free jet final height.

## 5. Final remarks

Particle migration in planar extrudate flows was studied. The suspension was described as a Newtonian liquid with a concentration-dependent viscosity, and shear-induced particle migration was modelled according to the diffusive flux

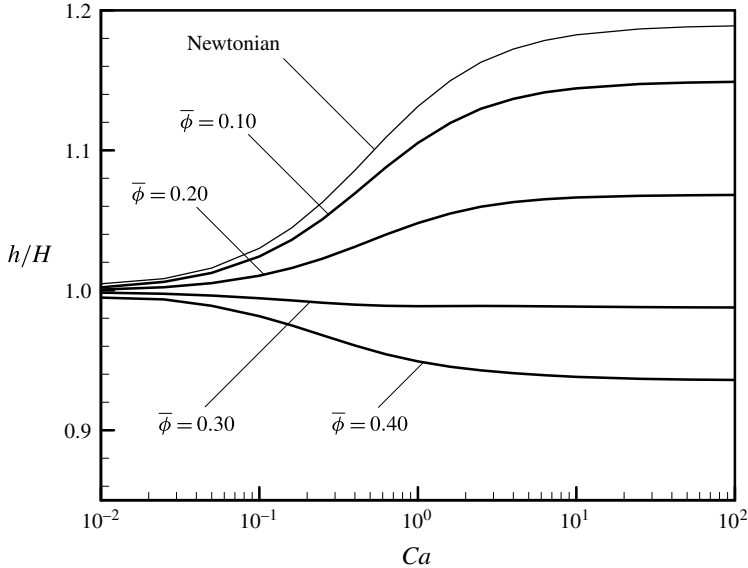


FIGURE 11. Effect of the capillary number on the free jet height.

model. The set of fully coupled, nonlinear differential equations was solved by the DEVSS-TG/SUPG finite element method together with the elliptic mesh generation method to capture the position of the free surface.

The results show that particle concentration distribution at the free-surface outflow is highly non-uniform, presenting higher concentration near the flow symmetry plane and lower concentration near the air–liquid interface. Particle migration affects the local viscosity and flow velocity, and thereby changes the suspension stress field near the channel exit. For a Newtonian liquid and dilute suspensions, die swell was observed. On the other hand, at high concentrations, a die contraction was observed. Here, this change in the free-surface curvature is related to the stress field variation caused by particle migration. The curvature of the free surface increases with the capillary number in order to balance the viscous force near the air–liquid interface. Therefore, for a Newtonian liquid and dilute suspensions, extrudate height increases with capillary number, whereas for concentrated suspensions, the extrudate height falls as capillary number increases. These results may explain the die-swell suppression observed in experiments of extrusion of particle-filled suspensions.

### Acknowledgements

This research was supported by the Brazilian Research Council (CNPq), the Carlos Chagas Filho Research Support Foundation (FAPERJ), and the Industrial Partnership for Research in Interfacial Materials & Engineering (IPrime, University of Minnesota). Additionally, we would like to thank our colleagues R. B. Rebouças (Department of Chemical & Environmental Engineering, Yale University) and L. H. P. da Cunha (Department of Mechanical Engineering, University of Brasília) for insightful discussions during this work.



## REFERENCES

- ABBOTT, J. R., GRAHAM, N., TETLOW, A. L., ALTOBELLI, S. A., FUKUSHIMA, E., MONDY, L. A. & STEPHENS, T. S. 1991 Experimental observations of particle migration in concentrated suspensions: Couette flow. *J. Rheol.* **35**, 773–797.
- AHMED, G. M. Y. & SINGH, A. 2011 Numerical simulation of particle migration in asymmetric bifurcation channel. *J. Non-Newtonian Fluid Mech.* **166**, 42–51.
- ALTOBELLI, S. A. & GIVLER, R. C. 1991 Velocity and concentration measurements of suspensions by nuclear magnetic resonance imaging. *J. Rheol.* **35**, 721–734.
- ARAL, B. K. & KALYON, D. M. 1997 Viscoelastic material functions of noncolloidal suspensions with spherical particles. *J. Rheol.* **41**, 599–620.
- BAJAJ, M., PRAKASH, J. R. & PASQUALI, M. 2008 A computational study of the effect of viscoelasticity on slot coating flow of dilute polymer solutions. *J. Non-Newtonian Fluid Mech.* **149**, 104123.
- BENJAMIN, D. F. 1994 Roll coating flows and multiple roll systems. PhD thesis, University of Minnesota, Minneapolis, MN, US.
- BIRD, R. B., ARMSTRONG, R. C. & HASSAGER, O. 1987 *Dynamics of Polymeric Liquids*, 1st edn. Wiley.
- BOLSTAD, J. H. & KELLER, H. B. 1986 A multigrid continuation method for elliptic problems. *J. Sci. Stat. Comput.* **7**, 1081–1104.
- BOYER, F., POULIQUEN, O. & GUAZZELLI, E. 2011a Dense suspensions in rotating-rod flows: normal stresses and particle migration. *J. Fluid Mech.* **686**, 5–25.
- BOYER, F., POULIQUEN, O. & GUAZZELLI, E. 2011b Unifying suspension and granular rheology. *Phys. Rev. Lett.* **107**, 188301.
- BRICKER, J. M. & BUTLER, J. 2006 Oscillatory shear of suspensions of noncolloidal particles. *J. Rheol.* **50**, 711–728.
- BUTLER, J. E. & BONNECAZE, R. T. 1999 Imaging of particle shear migration with electrical impedance tomography. *Phys. Fluids* **11**, 1982–1994.
- BUTLER, J. E., MAJORS, P. D. & BONNECAZE, R. T. 1999 Observations of shear-induced particle migration for oscillatory flow of a suspension within a tube. *Phys. Fluids* **11**, 2865–2877.
- CAMPANA, D. M., SILVA, L. D. V. & CARVALHO, M. S. 2017 Slot coating flows of non-colloidal particle suspensions. *AIChE J.* **63**, 1122–1131.
- CARVALHO, M. S. & KHESHGI, H. S. 2000 Low-flow limit in slot coating: theory and experiments. *AIChE J.* **46**, 1907–1917.
- CARVALHO, M. S. & SCRIVEN, L. E. 1997 Deformable roll coating flows: steady state and linear perturbation analysis. *J. Fluid Mech.* **339**, 143–172.
- CHANDRASEKHAR, S. 1961 *Hydrodynamic and Hydromagnetic Stability*. Oxford University Press.
- CHAPMAN, B. 1990 Shear-induced migration phenomena in concentrated suspensions. PhD thesis, University of Notre Dame, Notre Dame, IN, USA.
- CHOW, A. W., SINTON, S. W., IWAMIYA, J. H. & STEPHENS, T. S. 1994 Shear-induced migration in Couette and parallel-plate viscometers: NMR imaging and stress measurements. *Phys. Fluids* **6**, 2561–2576.
- CHRISTODOULOU, K. N. 1990 Computational physics of slide coating flow. PhD thesis, University of Minnesota, Minneapolis, MN, USA.
- CHU, W.-B., YANG, J.-W., WANG, Y.-C., LIU, T.-J. & GUO, J. 2006 The effect of inorganic particles on slot die coating of poly(vinyl alcohol) solutions. *J. Colloid Interface Sci.* **297**, 215–225.
- COUTURIER, E., BOYER, F., POULIQUEN, O. & GUAZZELLI, E. 2011 Suspensions in a tilted trough: second normal stress difference. *J. Fluid Mech.* **686**, 29–39.
- DBOUK, T., LOBRY, L. & LEMAIRE, E. 2013 Normal stresses in concentrated non-Brownian suspensions. *J. Fluid Mech.* **715**, 239–272.
- DODDS, S., CARVALHO, M. S. & KUMAR, S. 2009 Stretching and slipping of liquid bridges near plates and cavities. *Phys. Fluids* **21**, 092103.
- DODDS, S., CARVALHO, M. S. & KUMAR, S. 2011 Stretching liquid bridges with moving contact lines: the role of inertia. *Phys. Fluids* **23**, 092101.

- DODDS, S., CARVALHO, M. S. & KUMAR, S. 2012 The dynamics of three-dimensional liquid bridges with pinned and moving contact lines. *J. Fluid Mech.* **707**, 521–540.
- DUFF, I. S., ERISMAN, A. M. & REID, J. K. 1989 *Direct Method for Sparse Matrices*. Oxford University Press.
- EINSTEIN, A. 1911 Berichtigung zu meiner arbeit: Eine nene bestimmung der molekuldimension. *Ann. Phys.* **34**, 591–592.
- FURBANK, R. J. & MORRIS, J. F. 2004 An experimental study of particle effects on drop formation. *Phys. Fluids* **16**, 1777–1790.
- GADALA-MARIA, F. & ACRIVOS, A. 1980 Shear-induced structure in a concentrated suspension of solid spheres. *J. Rheol.* **24**, 799–814.
- GOVINDARAJAN, R., NOTT, P. R. & RAMASWAMY, S. 2001 Theory of suspension segregation in partially filled horizontally rotating cylinder. *Phys. Fluids* **13**, 3517–3520.
- GRAHAM, A. L. & ALTOBELLI, S. A. 1991 NMR imaging of shear-induced diffusion and structure in concentrated suspensions. *J. Rheol.* **35**, 191–201.
- GRAHAM, A. L., MAMMOLI, A. A. & BUSCH, M. B. 1998 Effects of demixing on suspension rheometry. *Rheol. Acta* **37**, 139–150.
- GUÉNETTE, R. & FORTIN, M. 1995 A new mixed finite element method for computing viscoelastic flows. *J. Non-Newtonian Fluid Mech.* **60**, 27–52.
- HAMPTON, R. E., MAMMOLI, A. A., GRAHAM, A. L., TETLOW, N. & ALTOBELLI, S. A. 1997 Migration of particles undergoing pressure-driven flow in a circular conduit. *J. Rheol.* **41**, 621–640.
- HAN, M., KIM, C., KIM, M. & LEE, S. 1999 Particle migration in tube flow of suspensions. *J. Rheol.* **43**, 1157–1174.
- HUSBAND, D. & GADALA-MARIA, F. 1987 Anisotropic particle distribution in dilute suspensions of solid spheres in cylindrical Couette flow. *J. Rheol.* **31**, 95–110.
- HUSBAND, D. M., MONDY, L. A., GANANI, E. & GRAHAM, A. L. 1994 Direct measurements of shear-induced particle migration in suspensions of bimodal spheres. *Rheol. Acta* **33**, 185–192.
- INGBER, M. S., GRAHAM, A. L., MONDY, L. A. & FANG, Z. 2009 An improved constitutive model for concentrated suspensions accounting for shear-induced particle migration rate dependence on particle radius. *Intl J. Multiphase Flow* **35**, 270–279.
- JIN, B. & ACRIVOS, A. 2004 Theory of particle segregation in rimming flow of suspensions containing neutrally buoyant particles. *Phys. Fluids* **16**, 641–651.
- KARNIS, A., GOLDSMITH, A. L. & MASON, S. G. 1966 The kinetics of flowing dispersions: concentrated suspensions of rigid particles. *J. Colloid Interface Sci.* **22**, 531–553.
- KHARCHENKO, S. B., DOUGLAS, J. F., OBRZUT, J., GRULKE, E. A. & MIGLER, K. B. 2004 Flow-induced properties of nanotube-filled polymer materials. *Nat. Mater.* **3**, 564–568.
- KIM, J. M., LEE, S. G. & KIM, C. 2008 Numerical simulations of particle migration in suspension flows: frame-invariant formulation of curvature-induced migration. *J. Non-Newtonian Fluid Mech.* **150**, 162–176.
- KOH, C. J., HOOKHAM, P. & LEAL, L. G. 1994 An experimental investigation of concentrated suspension flows in a rectangular channel. *J. Fluid Mech.* **266**, 1–32.
- KRISHNAN, G. P., BEIMFOHR, S. & LEIGHTON, D. 1996 Shear-induced radial segregation in bidisperse suspensions. *J. Fluid Mech.* **321**, 371–393.
- LEIGHTON, D. & ACRIVOS, A. 1987 The shear-induced migration of particles in concentrated suspensions. *J. Fluid Mech.* **181**, 415–439.
- LHUILIER, D. 2009 Migration of rigid particles in non-Brownian viscous suspension. *Phys. Fluid* **21**, 023302.
- LIANG, J. Z. 2010 Effects of diatomite on extrudate swell behavior of polypropylene composite melts. *J. Appl. Polym. Sci.* **118**, 385–389.
- LIU, C.-Y., VANDRE, E., CARVALHO, M. S. & KUMAR, S. 2016 Dynamic wetting failure in surfactant solutions. *J. Fluid Mech.* **789**, 285–309.
- LOIMER, T., NIR, A. & SEMIAT, R. 2002 Shear-induced corrugation of free interfaces in concentrated suspensions. *J. Non-Newtonian Fluid Mech.* **102**, 115–134.

- MILLER, R. M. & MORRIS, J. F. 2006 Normal stress-driven migration and axial development in pressure-driven flow of concentrated suspensions. *J. Non-Newtonian Fluid Mech.* **135**, 149–165.
- MIN, K. H. & KIM, C. 2010 Simulation of particle migration in free-surface flows. *AIChE J.* **56**, 2539–2550.
- MORRIS, J. F. 2001 Anomalous migration in simulated oscillatory pressure-driven flow of a concentrated suspension. *Phys. Fluids* **13**, 2457–2562.
- MORRIS, J. F. & BOULAY, F. 1999 Curvilinear flows of noncolloidal suspensions: the role of normal stresses. *J. Rheol.* **43**, 1213–1237.
- NICOLAS, M. 2002 Experimental study of gravity-driven dense suspension jets. *Phys. Fluids* **14**, 3570–3576.
- NORMAN, J. T., NAYAK, H. V. & BONNECAZE, R. T. 2005 Migration of buoyant particles in low-Reynolds-number pressure-driven flows. *J. Fluid Mech.* **523**, 1–35.
- NOTT, P. R. & BRADY, J. F. 1994 Pressure-driven flow of suspensions: simulation and theory. *J. Fluid Mech.* **275**, 157–199.
- NOTT, P. R., GUZZELLI, E. & POULIQUEN, O. 2011 The suspension balance model revisited. *Phys. Fluid* **23**, 043304.
- PASQUALI, M. & SCRIVEN, L. E. 2002 Free surface flows of polymer solutions with models based on the conformation tensor. *J. Non-Newtonian Fluid Mech.* **108**, 363–409.
- PHILLIPS, R. J., ARMSTRONG, R. C., BROWN, R. C., GRAHAM, A. L. & ABBOTT, J. R. 1992 A constitutive equation for concentrated suspensions that accounts for shear-induced particle migrations. *Phys. Fluids* **4**, 30–40.
- RAO, R. R., MONDY, L. A., BAER, T. A., ALTOBELLI, S. A. & STEPHENS, T. S. 2002 NMR measurements and simulations of particle migration in non-Newtonian fluids. *Chem. Engng Commun.* **189**, 1–22.
- REBOUÇAS, R. B., SIQUEIRA, I. R., DE SOUZA MENDES, P. R. & CARVALHO, M. S. 2016 On the pressure-driven flow of suspensions: particle migration in shear sensitive liquids. *J. Non-Newtonian Fluid Mech.* **234**, 178–187.
- ROMERO, O. J., SCRIVEN, L. E. & CARVALHO, M. S. 2006 Slot coating of mildly viscoelastic liquids. *J. Non-Newtonian Fluid Mech.* **138**, 63–75.
- ROMERO, O. J., SUSZYNSKI, W. J., SCRIVEN, L. E. & CARVALHO, M. S. 2004 Low-flow limit in slot coating of dilute solutions of high molecular weight polymer. *J. Non-Newtonian Fluid Mech.* **118**, 137–156.
- SANTAMARÍA-HOLEK, I. & MENDOZA, C. I. 2010 The rheology of concentrated suspensions of arbitrarily-shaped particles. *J. Colloid Interface Sci.* **346**, 118–126.
- DE SANTOS, J. M. 1991 Two-phase cocurrent downflow through constricted passages. PhD thesis, University of Minnesota, Minneapolis, MN, USA.
- SINGH, A., NIR, A. & SEMIAT, R. 2006 Free-surface flow of concentrated suspensions. *Intl J. Multiphase Flow* **32**, 775–790.
- SINTON, S. A. & CHOW, A. 1991 NMR flow imaging of fluids and solid suspensions in Poiseuille flow. *J. Rheol.* **35**, 735–772.
- SIQUEIRA, I. R., REBOUÇAS, R. B. & CARVALHO, M. S. 2017a Migration and alignment in the flow of elongated particle suspensions through a converging-diverging channel. *J. Non-Newtonian Fluid Mech.* **243**, 56–63.
- SIQUEIRA, I. R., REBOUÇAS, R. B. & CARVALHO, M. S. 2017b Particle migration and alignment in slot coating flows of elongated particle suspensions. *AIChE J.*; Available online at Wiley Online Library – doi:[10.1002/aic.15653](https://doi.org/10.1002/aic.15653).
- SNOOK, B., BUTLER, J. E. & GUZZELLI, E. 2016 Dynamics of shear-induced migration of spherical particles in oscillatory pipe flow. *J. Fluid Mech.* **786**, 128–153.
- STICKEL, J. J. & POWELL, R. L. 2005 Fluid mechanics and rheology of dense suspensions. *Annu. Rev. Fluid Mech.* **37**, 129–149.
- SUBIA, S. R., INGBER, M. S., MONDY, L. A., ALTOBELLI, S. A. & GRAHAM, A. L. 1998 Modelling of concentrated suspensions using a continuum constitutive equation. *J. Fluid Mech.* **373**, 193–219.

- SZADY, M. J., SALAMON, T. R., LIU, A. W., ARMSTRONG, R. C. & BROWN, R. A. 1995 A new mixed finite element method for viscoelastic flows governed by differential constitutive equations. *J. Non-Newtonian Fluid Mech.* **59**, 215–243.
- TADROS, T. F. 2011 *Rheology of Dispersions: Principles and Applications*. Wiley.
- TADROS, T. F. 2017 *Suspension Concentrates: Preparation, Stability and Industrial Applications*. Walter De Gruyter.
- TANNER, R. I. 1985 *Engineering Rheology*, 1st edn. OUP.
- TETLOW, N., GRAHAM, A. L., INGBER, M. S., RUBIA, S. R., MONDY, L. A. & ALTABELLI, S. A. 1998 Particle migration in a Couette apparatus: experiment and modeling. *J. Rheol.* **42**, 307–327.
- TIMBERLAKE, B. D. & MORRIS, J. F. 2002 Concentration band dynamics in free-surface Couette flow of a suspension. *Phys. Fluids* **14**, 1580–1589.
- TIMBERLAKE, D. M. & MORRIS, J. F. 2005 Particle migration and free-surface topography in inclined plane flow of a suspension. *J. Fluid Mech.* **538**, 309–341.
- TIRUMKUDULU, M., MILEO, A. & ACRIVOS, A. 2000 Particle segregation in monodisperse sheared suspension in partially filled rotating horizontal cylinder. *Phys. Fluids* **12**, 1615–1618.
- TIRUMKUDULU, M., TRIPATHI, A. & ACRIVOS, A. 1999 Particle segregation in monodisperse sheared suspension. *Phys. Fluids* **11**, 507–509.
- TJIPTOWIDJOJO, K. & CARVALHO, M. S. 2011 Operability limits of slide coating. *Chem. Engng Sci.* **66**, 5077–5083.
- VANDRE, E., CARVALHO, M. S. & KUMAR, S. 2012 Delaying the onset of dynamic wetting failure through meniscus confinement. *J. Fluid Mech.* **707**, 496–520.
- VANDRE, E., CARVALHO, M. S. & KUMAR, S. 2013 On the mechanism of wetting failure during fluid displacement along a moving substrate. *Phys. Fluids* **25**, 102103.
- VANDRE, E., CARVALHO, M. S. & KUMAR, S. 2014 Characteristics of air entrainment during dynamic wetting failure along a planar substrate. *J. Fluid Mech.* **747**, 119–140.
- ZARRAGA, I. E., HILL, D. A. & LEIGHTON, D. T. 2000 The characterization of the total stress of concentrated suspensions of non-colloidal spheres in Newtonian fluids. *J. Rheol.* **44**, 185–220.